

PCCP

Accepted Manuscript



This is an *Accepted Manuscript*, which has been through the Royal Society of Chemistry peer review process and has been accepted for publication.

Accepted Manuscripts are published online shortly after acceptance, before technical editing, formatting and proof reading. Using this free service, authors can make their results available to the community, in citable form, before we publish the edited article. We will replace this *Accepted Manuscript* with the edited and formatted *Advance Article* as soon as it is available.

You can find more information about *Accepted Manuscripts* in the [Information for Authors](#).

Please note that technical editing may introduce minor changes to the text and/or graphics, which may alter content. The journal's standard [Terms & Conditions](#) and the [Ethical guidelines](#) still apply. In no event shall the Royal Society of Chemistry be held responsible for any errors or omissions in this *Accepted Manuscript* or any consequences arising from the use of any information it contains.



Journal Name

ARTICLE

Fundamental insights of electronic structure on zigzag MoS₂ nanoribbons

Shansheng Yu*^a and Weitao Zheng^aReceived 00th January 20xx,
Accepted 00th January 20xx

DOI: 10.1039/x0xx00000x

www.rsc.org/

The structural and electronic properties of zigzag MoS₂ nanoribbons are investigated using first-principles density functional theory. Our models are motivated by the experimental observations, in which both Mo edges are terminated by S atoms. Our calculations show that the edge can introduce some extra states into energy gap, which lead nanoribbons to exhibiting a metallic characteristic. Such extra states around the Fermi level are flat or dispersed. Through a detailed analyses, we identify and discriminate them based on the major contributors. By applying an external transverse electric field, E_{ext} , the extra states around the Fermi level can shift apparently, especially for those attributed to Mo-edge atoms. It can be explained by the charge redistribution in the MoS₂ nanoribbons due to E_{ext} . In addition, the nanoribbon can be changed from metal to n/p-type semiconductor according to different edge hydrogenation. After full edge hydrogenation, we observe a characteristic of anti-bonding orbitals between H and S atoms at the Mo-edge. Interestingly, the energy of anti-bonding orbitals and electric conductivity of nanoribbon can be tailored by E_{ext} . The results suggest a strategy controlling the performance of MoS₂ for hydrogen evolution.

Introduction

Graphene is the first example of true two-dimensional (2D) single-layer atomic crystal in 2004, which has some unique properties and promising applications.¹ The intensive studies on graphene have motivated researchers to develop new 2D materials.^{2,3} The representative examples for 2D materials other than graphene are monolayers of *h*-BN, dichalcogenides (such as MoS₂ and NbSe₂), BC₃, silicene, phosphorene, MXene, arsenene, antimonene, complex oxides (such as Bi₂Sr₂CaCu₂O_x), and coordination polymers.⁴⁻¹⁰ These novel materials have rather fantastic physical properties with potential applications. For example, BN nanosheets are highly insulating, and exhibit superb chemical, thermal, and oxidation stability. Although silicene possesses graphene-like structures, the pseudo-Jahn-Teller (PJT) distortion occurs and leads to the buckling in silicenes.⁹ The spin orbit coupling of silicene is stronger than that of graphene, which is more applicable as spintronic devices. MoS₂ nanosheets were explored as high-temperature solid lubricants, nanoelectronics, electrode materials, and catalysts. The atomic structure of monolayer MoS₂ is two S-layers sandwiching a Mo-layer, and the atoms in layers are hexagonally packed, which was found to be a direct band gap

semiconductor.¹¹ Due to interesting physical and chemical properties, it has attracted a growing interest from researchers.¹²

Currently, studies extend to the low-dimensional structures of MoS₂ such as nanoribbon.¹³⁻¹⁷ A breakthrough in fabricating ultranarrow MoS₂ nanoribbon was reported in 2010, in which the MoS₂ nanoribbon was encapsulated into a carbon nanotube.¹⁸ Because the electronic and magnetic properties of nanoribbon can be modified by manipulating its edges, MoS₂ nanoribbon is believed to have wide application in nanoelectronics devices.¹⁹⁻²² Similar to graphene nanoribbon, MoS₂ nanoribbon can be classified by atomic geometry along the edge, viz., zigzag or armchair, which electronic and magnetic properties are also dependent on edge structures.^{15,23-26} Armchair MoS₂ nanoribbon is semiconducting, regardless of H-saturation. Its electronic properties are weakly dependent on the nanoribbon width. With its width increasing, its band-gap converges to a value smaller than that of MoS₂ monolayer.^{15,24} However, zigzag MoS₂ nanoribbon exhibits metallic behavior.^{15,23-25} Both experiment and theory show that the zigzag MoS₂ nanoribbons are generally more stable than the armchair MoS₂ ones.¹⁸ In 2012, Chen et al. found that zigzag MoS₂ nanoribbons had a remarkably enhanced Li adsorption and at the same time preserved the high Li mobility in comparison with MoS₂ nanosheets.²⁷ Such argument will motivate experimental studies on zigzag MoS₂ nanoribbons as cathode materials of Li-ion batteries.

The electronic properties of MoS₂ nanoribbons can be manipulated by the application of strain, defects, adsorption, doping, and so on.^{17,28-31} An external electric field has been demonstrated to can effectively tune the electronic structures

^a Department of Materials Science, Key Laboratory of Mobile Materials, Ministry of Education, State Key Laboratory of Superhard Materials, Jilin University, Changchun, 130012, China. E-mail: yuss@jl.u.edu.cn

†Electronic Supplementary Information (ESI) available: The energy bands of MoS₂ monolayer. The transition state search from NR-2 to NR-2'. The calculated band structures of NR-1 and NR-2 as a function of a static external electric field. Total density of states for hydrogen passivated NR-1 under $E_{ext}=-2.5$ V/nm and 2.5 V/nm. See DOI: 10.1039/x0xx00000x

of graphene nanoribbon.³² This also can apply to modulation of MoS₂ nanoribbon. It is found that the band-gap of armchair MoS₂ nanoribbon can be tuned by an external electric field, and metal-insulator transition occurs at a critical electric field.^{16,33} The electronic properties of zigzag MoS₂ nanoribbon are also sensitive to electric field, which stem from the energy-level shifts induced by an internal electric polarization and the competing covalent/ionic interactions.¹⁷ The band-gap of the bilayer MoS₂ monotonically decreases with an increasing vertical electric field, in which the semiconductor-to-metal transition occurs.³⁴ For graphene-MoS₂ heterojunction, though the external vertical electric field has little influence on the bandgap of MoS₂, the charge transfer, the Schottky barrier, and the work function can be controlled.³⁵ Currently, researchers mostly focus on band-gap of armchair MoS₂ nanoribbon, whereas an electric field effects on zigzag MoS₂ nanoribbon is considered with a relatively small volume. Especially, the variation of electronic band with external electric field is rarely explored.

In this paper, we consider the structures of nanoribbon originating from experimental results. According to the high-angle annular dark field (HAADF) images, the needle-like MoS₂ nanowires could be stabilized by a strong sulfidizing atmosphere.^{36,37} Particularly, the ultranarrow MoS₂ nanoribbons with uniform width and smooth edges were obtained in carbon nanotubes as templates.¹⁸ According to the high-resolution transmission electron microscopy (HR-TEM) and density functional theory (DFT) calculations, the Mo-edge of MoS₂ nanoribbons tends to be half-saturated by S atoms, while the S-edge prefers to be bare. Therefore, we proposed a simple model which edges were saturated with sulfur to compensate the dangling bonds. In addition, MoS₂ nanowires with such morphology may be related to potential catalytic activity.^{36,38,39} It is well known that the one-dimensional edge sites along the layers for MoS₂ are responsible for the catalytic activity in the hydrogen evolution reaction (HER) while the basal plane of MoS₂ is catalytically inactive.^{36,40} In order to improve the HER performance, the various strategies for increasing number of active sites and prompting catalytic efficiency are designed, such as doping and hybrid with other materials.⁴¹⁻⁴⁴ In order to engineer better their applications, it is required to deeply understand the electronic structures of these MoS₂ nanoribbons. Using first-principles DFT, we have systematically investigated their electronic structures, and identification of energy bands around the Fermi level as well as external electric field effects on their electronic structures.

Methods and Models

In this work, the calculations of geometrical optimization and electronic structures were performed using DFT by Dmol3 code.⁴⁵ In the DFT calculations, the all-electron Kohn–Sham wavefunctions were expanded in the double numerical polarized atomic orbital basis, and the generalized gradient approximation with the Perdew–Burke–Ernzerh of describing the exchange and correlation energy was employed.⁴⁶ Self-

consistent field procedure was done until the change of energy was less than 10⁻⁶ Hartree, and the geometrical optimization of the structure was done with an energy convergence criterion of 10⁻⁵ Hartree. Long range nonlocal effects were taken into account by applying van der Waals dispersion corrections through the DFT-D scheme with Grimme parameters,⁴⁷ whose S₆=0.75. In atomic parameters, C₆ for H, S and Mo is chosen to be 1.451, 57.729 and 255.687 eVÅ⁶, and the vdW radius R⁰ is set as 1.001, 1.683 and 1.639 Å, respectively. For energy band calculations, the sampling of was carried out with 0.001Å⁻¹ between consecutive *k*-points on the reciprocal space path.

The dynamic stability of new structures had also been examined by the molecular dynamics using the Dmol3 code.⁴⁵ The constant temperature and volume (NVT) ensemble was conducted with time steps of 5 fs for a total simulation time of 10 ps at 1000 K. In addition, the linear synchronous transit (LST) and quadratic synchronous transit (QST) were performed to find a transition-state structure. Calculations using CASTEP⁴⁸ code were also employed to understand the behavior of electronic orbitals near the Fermi level.

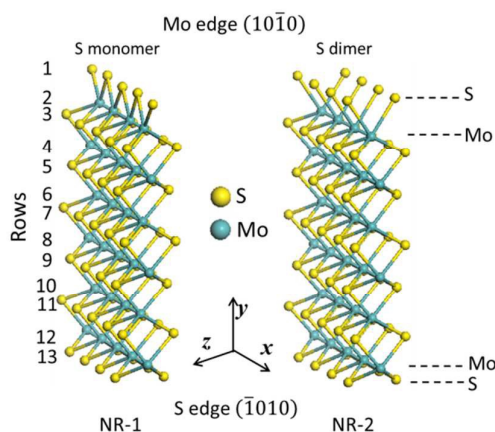


Fig. 1 Perspective view of the MoS₂ nanoribbons. The width of nanoribbon is the thirteen rows, and the rows from the first row (Mo-edge) to the thirteenth row (S-edge) are labelled by Arabic numerals.

The experimental in-plane lattice constant of 3.16Å for the in-plane unit cell of MoS₂ monolayer has been used. Optimizing MoS₂ monolayer, we obtained a semiconductor with a direct gap of 1.81 eV in ESI Fig. S1, which is in a good agreement with experimental result.¹¹ The quasi-one dimensional zigzag nanoribbon can be cut from a perfect MoS₂ monolayer along the zigzag direction. According to experimental HAADF and HR-TEM images of needle-like MoS₂ nanowires and ultranarrow MoS₂ nanoribbons, the Mo-edge is adsorbed with sulfur.^{18,36} The width of nanoribbon we chose is thirteen rows including six rows of Mo and seven rows of S, as shown in Fig. 1. A one-dimensional periodic boundary condition is applied along *x*-direction. The periodically repeating tetragonal unit cell dimension in *x*-direction is 6.32 Å containing two Mo atoms, in *y*-direction 50 Å and in *z*-direction 50 Å. A vacuum region is enough to ensure negligible interaction between the infinite nanoribbon and its periodic images.

According to experimental HAADF images of needle-like MoS₂ nanowires,³⁶ two edge configurations are considered in our models. For the Mo-edge (10 $\bar{1}0$), the degrees of S-coverage are 50% and 100%, respectively, which correspond to S-monomer and S-dimer edge configurations. For the S-edge ($\bar{1}010$), we only consider one edge configuration (100% of sulfur coverage). Therefore, two models of sulfur terminated were constructed in Fig. 1, which are labelled by NR-1 and NR-2, respectively.

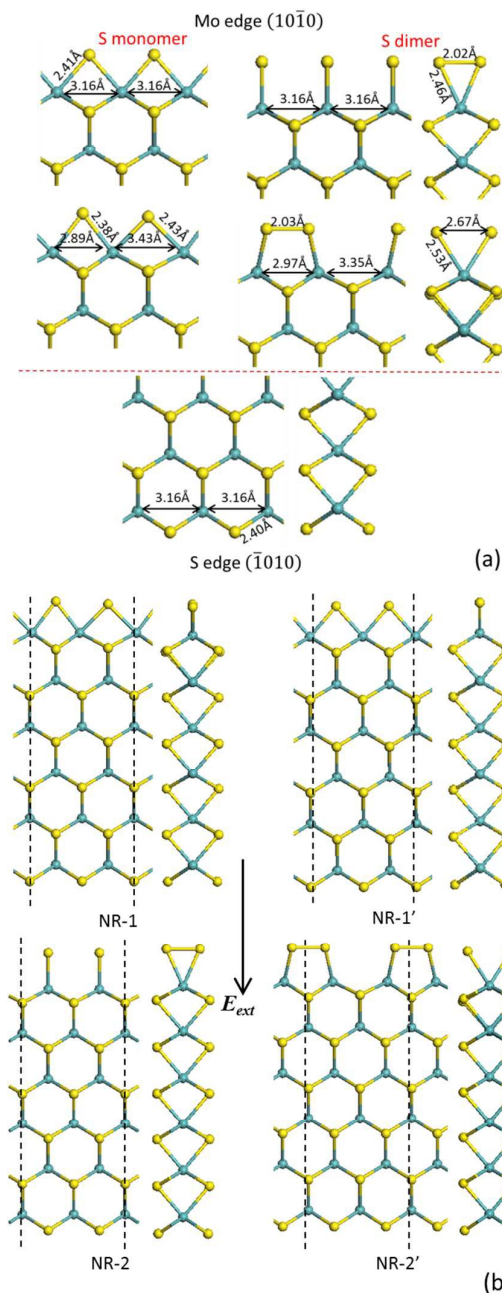


Fig. 2. (a) The enlarged view of geometric fragments of Mo-edge (top) and S-edge (down) including bond lengths (in Å). (b) The geometric structures of the MoS₂ nanoribbons, in which the dashed lines mark the dimension of the unit cell in the x-direction.

Results and discussion

Geometric structures

After DFT geometric relax, compared with S-Mo bond (2.43 Å) of MoS₂ monolayer, the large distortions occur at the edge due to edge effects in Fig. 2(a). At the S-edge ($\bar{1}010$), the length of S-Mo bond is shortened to 2.40 Å. Noticeably, at the Mo-edge (10 $\bar{1}0$), there exist two different configurations for each S-monomer and S-dimer edge configurations. Consequently, four models will occur in Fig. 2(b). For S-monomer edge configuration, in the upper left case of Fig. 2(a), the length of S-Mo bond (2.41 Å) slightly is reduced, and distances between Mo atoms are equal. This model is labelled by NR-1'. However, in another case labelled by NR-1, we observe that a geometric distortion presents, in which the Mo atoms at the Mo-edge are paired, for example the distance between Mo atoms alternately is 2.89 Å and then 3.43 Å. In order to describe conveniently, terminated S atom facing toward distance of 2.89 Å is labelled by S1, and another is labelled by S2. For S-dimer edge configuration, one model is labelled by NR-2, in the upper right case of Fig. 2(a), in which the distances between Mo edge-atoms are equal (3.16 Å), and every one Mo-atom is terminated by one S-dimer, resulting in a triangle at the Mo-edge. However, in another case labelled by NR-2', the Mo-edge is characterized by one terminated S-dimer per two Mo-atom, leading to a quadrangle at the Mo-edge. Like NR-1, the Mo atoms are also paired at the Mo-edge in NR-2'.

We start to study the relative stability of the different models. Since these structures have the same chemical compositions, the cohesive energy per atom can provide a suitable measure for the comparison of their relative stability. The per-atom cohesive energy (E_{coh}) is defined as

$$E_{coh} = [E_{tot} - \sum_i n_i E_i] / N \quad (i = S, Mo) \quad (1)$$

where E_{tot} and E_i are total energies of a system and of individual elements present within the same cell, respectively. n_i is the number of S or Mo atom, and N is the total number of atoms in a cell. The model with a higher negative cohesive energy results in a higher structural stability. The calculations results show that NR-1 and NR-2' have the highest and lowest negative values of E_{coh} , respectively. $|E_{coh}|$ of NR-1 is slightly larger than that of NR-1' ($E_{coh}(NR-1) - E_{coh}(NR-1') = -2.1$ meV/atom), while $|E_{coh}|$ of NR-2 or NR-2' decreases by 65.0 meV/atom or 77.4 meV/atom compared with that of NR-1. According to HAADF and HR-TEM images in the experiments,^{18,36} the models of NR-1 and NR-2 were proposed. Combined with them, they provide us a reference frame for comparison. In addition, we should consider that the experimentally obtained nanoribbons depend on the experimental procedures, and may be not essentially the thermodynamically most favorable.

The two models of NR-1 and NR-1' are not exactly degenerate but are very close in energy. The symmetry of NR-1 is lower than that of NR-1'. It is well known that silicene and germanene are in favor of buckling induced lowering of symmetry, which origin is PJT distortion.^{9,49} Therefore, we think that such phenomenon, the lowering in symmetry from NR-1' to NR-1, may be related to PJT distortion. When the

degree of S-coverage is 50% at the Mo-edge, the bonding configuration of Mo atom at the edge is distorted, which is different from that of Mo atom in the inner. Thus, for Mo atom at the edge, the ground and excited states can rather easily undergo interacting by vibronic coupling. Such the changes of bonding configuration will influence nuclear configuration. In fact, for NR-1', the periodically repeating unit cell dimension in *x*-direction is 3.16 Å containing one Mo atom. When the unit cell dimension in *x*-direction doubles, the model of NR-1' we considered can be obtained, as seen in Fig. 2. However, after DFT geometric relax of this NR-1', a geometric distortion occurs at the Mo-edge, and then NR-1' will spontaneously be transformed into NR-1. Therefore, the model of NR-1' is physically meaningless configuration. On the contrary, the models of NR-2 and NR-2' are both stable configurations, which lie local energy minimum on the potential energy surface. Using LST/QST tools, a transition-state structure between them is found, which is shown in ESI Fig. S2. The results show that the energy barrier from NR-2 to NR-2' is 28.6 kcal/mol. In topography, a triangle is more stable than a quadrangle. Importantly, at the Mo-edge, it is noted that the bond (2.46 Å) between Mo atom and terminated S atom for NR-2 is stronger than that (2.53 Å) for NR-2'. Imagine if this bond for NR-2' could be shorten, the bond (2.03 Å) of S dimer would tend to elongate. The energy required for elongation of S-S bond is larger than that released for shrinkage of S-Mo bond. Therefore, we suggest that NR-2 can be more stable than NR-2'.

Their dynamic stabilities have also been examined by the molecular dynamics simulations. We considered the supercells of NR-1, NR-2 and NR-2' systems by doubling their unit cell of dimension in *x*-direction. After 10 ps molecular dynamics simulations, they are basically stable and have a slight distortion (see ESI, Fig. S3). Therefore, it is possible that NR-1, NR-2 and NR-2' systems would exist stably.

Electronic properties

Although the model of NR-1' is not stable structure, its electronic structures are required to help understanding those of NR-1. As their total densities of states (TDOS) are shown in Fig. 3(a), they both exhibit metallic characteristic and have a sharp state marked by arrows at the Fermi level. In addition, we find that one dispersed band goes across the Fermi level for NR-1' while counterpart of NR-1 is almost flat in Fig. 3(b), which induces that the sharp state of NR-1 is stronger than that of NR-1' in Fig. 3(a). These behaviors are different from that of semiconducting MoS₂ monolayer in ESI Fig. S1. We consider that edge-atoms will introduce some extra electronic states into band-gap. Therefore, the local densities of states (LDOS) are also calculated for edge atoms in Fig. 3(c). For NR-1', the sharp state at the Fermi level is mainly contributed from S atoms at the S-edge, and the electronic states coming from S and Mo atoms at the Mo-edge are dispersed across the Fermi level. For NR-1, the sharp state is derived mainly from S atoms at the S-edge and Mo atom at the Mo-edge, although there are smaller contributions from terminated S atoms at the Mo-edge. As shown in the inset of Fig. 3(a), the electronic orbitals

of the sharp state in the real space also exhibit a similar distribution to above description. After analysis and comparison, we can indicate that the bands marked by asterisk are introduced by S-edge atoms, and the bands marked by pound sign are attributed to Mo-edge atoms in Fig. 3(b). Both of these models have four similar bands circled by dashed line with a slight different energy. Three bands belong to S-edge atoms, and the fourth band is introduced by Mo atoms at Mo-edge. We can reasonably think that, for bands introduced by S-edge, two almost flat-bands at the Fermi level mainly stem from S atoms, and one dispersed band above the Fermi level is induced by Mo atoms. In addition, one band labelled by arrows at the Fermi level can be largely attributed to Mo atoms at the Mo-edge. Due to a geometric distortion at the Mo-edge during the structural optimization, the dispersed band across the Fermi level in NR-1' is suppressed and transformed into almost flat-band in NR-1. We expect that this geometric distortion (the pairing of the Mo atoms) at the Mo-edge can lead to prominent edge-states character, such as for needle-like MoS₂ nanopipes.³⁶ These results are also consistent with Chen's calculations where the prominent mid-gap states induced by edge atoms appear near the Fermi level, which can be expected to enhancing Li adsorption.²⁷

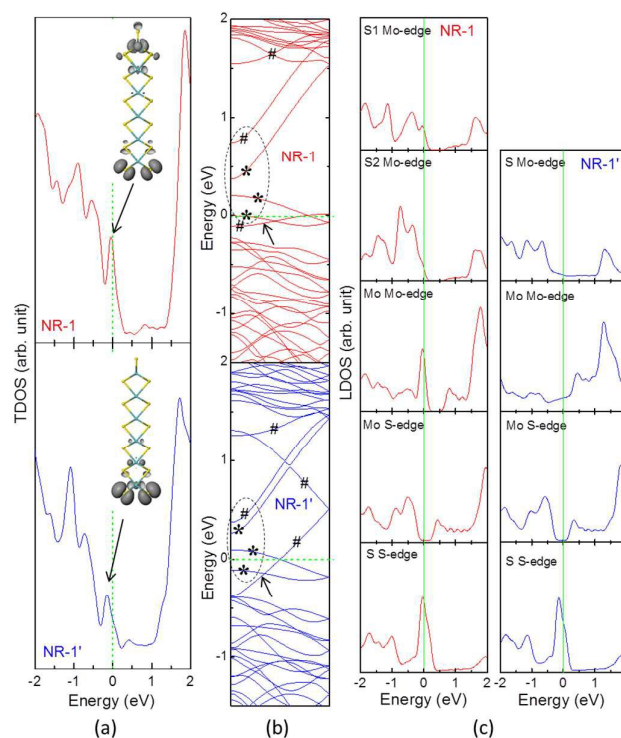


Fig. 3. (a) TDOS of NR-1 and NR-1', the sharp state is marked by arrows. Inset: the electronic orbitals of corresponding sharp states. (b) Energy bands of NR-1 and NR-1'. (c) LDOS of NR-1 and NR-1' for edge-atoms. The Fermi level is set as zero.

The electronic structures of NR-2 and NR-2' are calculated in Fig. 4. They also present the metallic characteristic and have a sharp state marked by arrows near the Fermi level in Fig. 4(a). As above description, we denote some bands near the Fermi level introduced by S-edge atoms by asterisk and attributed to

Mo-edge atoms by pound sign in Fig. 4(b). Noticeably, the bands introduced by S-edge atoms are similar to those of NR-1(1'), whose sites only move a little towards low energy zone. The sharp states at the Fermi level are mainly contributed from S atoms at the S-edge, which also can be verified by the electronic orbitals in the inset of Fig. 4(a). However, the appearances of bands induced by Mo-edge atoms are different from those of NR-1(1'). In the dashed circle, although one band marked by pound sign comes from Mo atoms at the Mo-edge, it extends down and goes across the Fermi level for NR-2(2') while that band extends up and lies above the Fermi level for NR-1(1'). The electronic structures of NR-2 are compared with those of NR-2' in Fig. 4(b)(c). We find that the terminated S-dimers at the Mo-edge largely induce difference between their electronic structures. The electronic states introduced by S-dimer are dispersed and very wide across the Fermi level for NR-2. However, the corresponding states are discrete and localized on both sides of Fermi level for NR-2', and it seems like an electron-hole symmetry. We suggest that the topography at the Mo-edge can cause electronic states contributed from terminated S atoms to be localized.

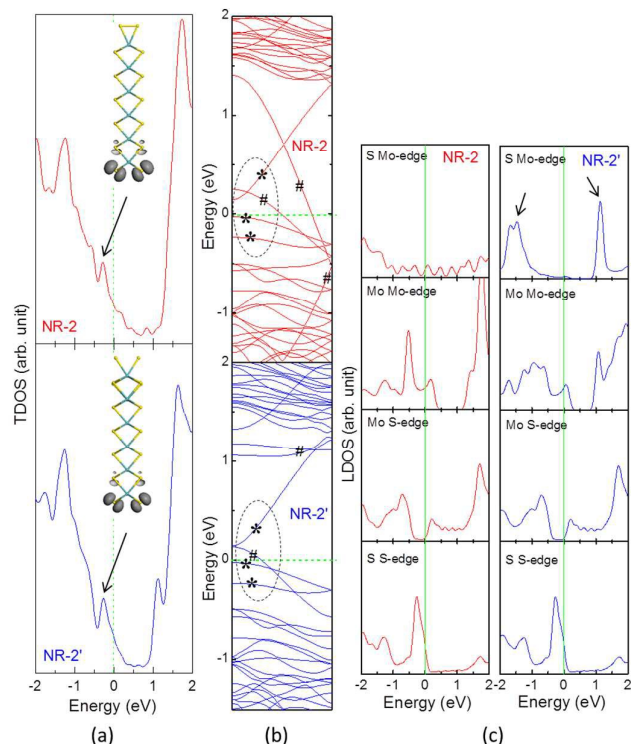


Fig. 4. (a) TDOS of NR-2 and NR-2', the sharp state is marked by arrows. Inset: the electronic states of corresponding sharp states. (b) Energy bands of NR-2 and NR-2'. (c) LDOS of NR-2 and NR-2' for edge-atoms. The Fermi level is set as zero.

Electric field effects

We now discuss the response of their electronic structures to a static external electric field (E_{ext}). The models of NR-1 and NR-2 are considered due to their stability. A uniform E_{ext} is applied across the MoS₂ nanoribbons width. Compared with their electronic structures under $E_{ext}=0.0$ V/nm in Fig. 3 and Fig. 4, it

is worth noting that the bands labelled by arrows are visibly sensitive to E_{ext} in Fig. 5, and their energies vary greatly with E_{ext} . Many band structures under other E_{ext} also can be seen in ESI Fig. S4. We turn our attention now to the electronic states around the Fermi level. It is observed that the electronic states near the Fermi level shift up or down when the positive or negative E_{ext} is applied. Particularly, the states introduced by Mo-edge atoms are more greatly altered than those contributed from S-edge atoms. These behaviors are different from those of graphene nanoribbons. It seems like that the negative/positive E_{ext} can inject electrons/holes into MoS₂ nanoribbons. Additionally, we have calculated their electronic structures as a function of ribbon width under E_{ext} in ESI Fig. S5. It is found that their electronic structures with various widths are robust except the flat band at the Fermi level for NR-1. The flat band attributed from Mo-edge atoms is becoming dispersed apparently with decreasing width when the positive E_{ext} is applied.

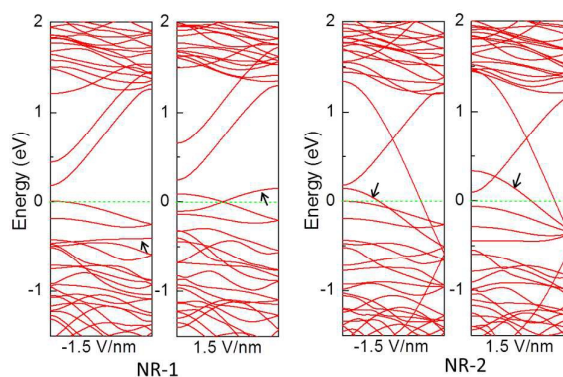


Fig. 5. Energy bands under E_{ext} for NR-1 and NR-2 are exhibited. The Fermi level is set as zero.

The E_{ext} on MoS₂ nanoribbons will result in the charge redistribution which may give important qualitative information about the nature of such interesting doping behaviors by E_{ext} . A Mulliken population analysis is considered, by means of which we can estimate the total Mulliken charge on each atom. In Fig. 6, we exhibit the profile of the charge distribution and the integrated charge per atom as a function of the row number. The charge distribution is shown as linear charge densities $\lambda(r)$ presenting the average value of charge per atom at the r row. The integrated charge is described as total net charge per atom in a range of rows from r_1 to r_2 :

$$IC(r_2) = [1/N] \sum_{r=r_1}^{r_2} \lambda(r) \times n_r \quad (2)$$

where n_r is the number of atoms at the r row, and N is the number of atoms summed over rows from r_1 to r_2 . We focus on the variation of integrated charge per atom at the regions from edges to inner, which is from $r_1=1$ to r_2 ($r_2=1, 2, 3, \dots, 6$), and another is from $r_1=13$ to r_2 ($r_2=13, 12, 11, \dots, 7$).

Figure 6 shows that the charge distribution oscillates with $\lambda(r)$ alternating in sign under $E_{ext}=0.0$ V/nm. $\lambda(r)$ at the odd/even-numbered row presents negative/positive value in accord with the characteristic of MoS₂. The interaction between the Mo and S atoms is the competing ionic and covalent bonding characters, especially for those at the

edges.⁵⁰ Its integrated charge per atom is calculated as shown in the upper inset of Fig. 6. It is discernable that the amplitude of oscillation is enlarged when closing to nanoribbon edge. Thus, we expect the existence of edge effects stemming from the broken bonds and bond contraction at the edges.⁵¹ Note also that the oscillation approaching Mo-edge is slightly more violent than that approaching S-edge. It may be due to that the geometric distortion is larger at the Mo-edge than that at the S-edge. The relative change of the covalent/ionic bonding characters at such distortion would lead to more accumulation of charge at the Mo-edge than that at the S-edge.¹⁷

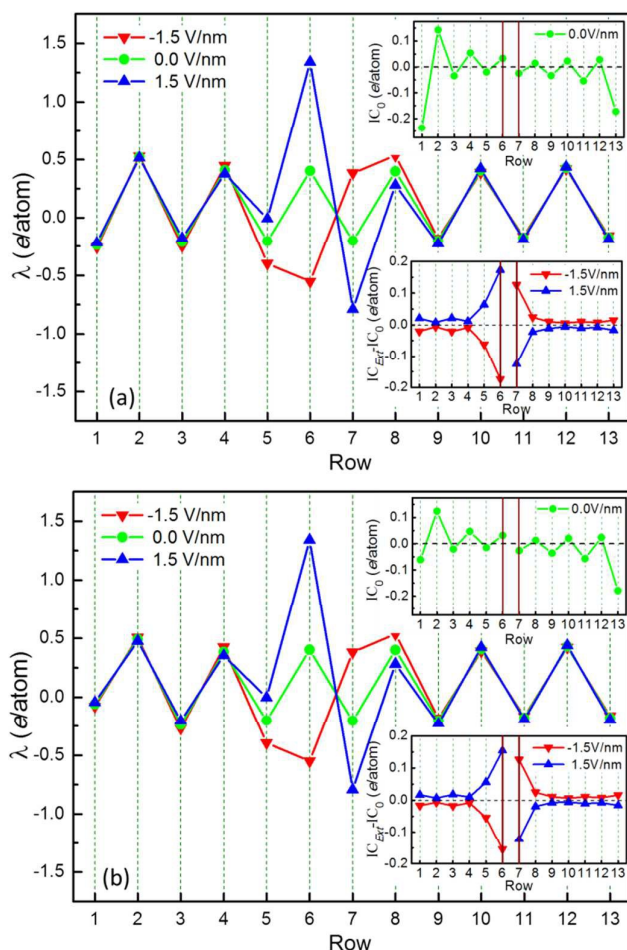


Fig. 6. Charge distribution for (a) NR-1 and (b) NR-2 under $E_{ext} = -1.5$ V/nm (red down-triangles), 0.0 V/nm (green circles), and 1.5 V/nm (blue up-triangles). Upper inset: the integrated charge per atom under $E_{ext} = 0.0$ V/nm; Lower inset: the differentiation between the integrated charges per atom under $E_{ext} = 0.0$ V/nm and $E_{ext} = -1.5/1.5$ V/nm.

When E_{ext} is applied, as the charge distributions shown, we observe that the violent oscillation occurs at the middle of ribbon, which seems like the outbreak of oscillatory source to propagate from inner to edge. Noticeably, the negative E_{ext} causes the oscillation to reverse the sign at the 6th and 7th rows while the positive E_{ext} does not. Because such additional oscillatory source can induce the charge redistribution in the nanoribbon, we expect that the additional charges from oscillatory source will be poured from inner into edges.

Subtract $\lambda(r)$ under $E_{ext} = 0.0$ V/nm from that under $E_{ext} = -1.5$ or 1.5 V/nm and we have their difference values, viz., additional charges. Putting these values into eqn (2), we can obtain the integrated additional charge induced by oscillatory gain under $E_{ext} = -1.5$ or 1.5 V/nm relative to that under $E_{ext} = 0.0$ V/nm. Their plots are shown in the lower inset of Fig. 6. At the left panel, the integrated additional charges induced by the negative/positive E_{ext} are all negative/positive values, whereas the signs of these values are reversed at the right panel. Thus, the whole systems can keep electric neutrality. We observe that the oscillation at the left panel is more violent than that at the right panel. Importantly, the amplitude near the Mo-edge is larger than that near the S-edge. Consequently, the relatively shallower states as a whole exhibit the electrons or holes doping behaviors by the negative or positive E_{ext} , and the electronic states introduced by Mo-edge atoms are especially altered greatly.

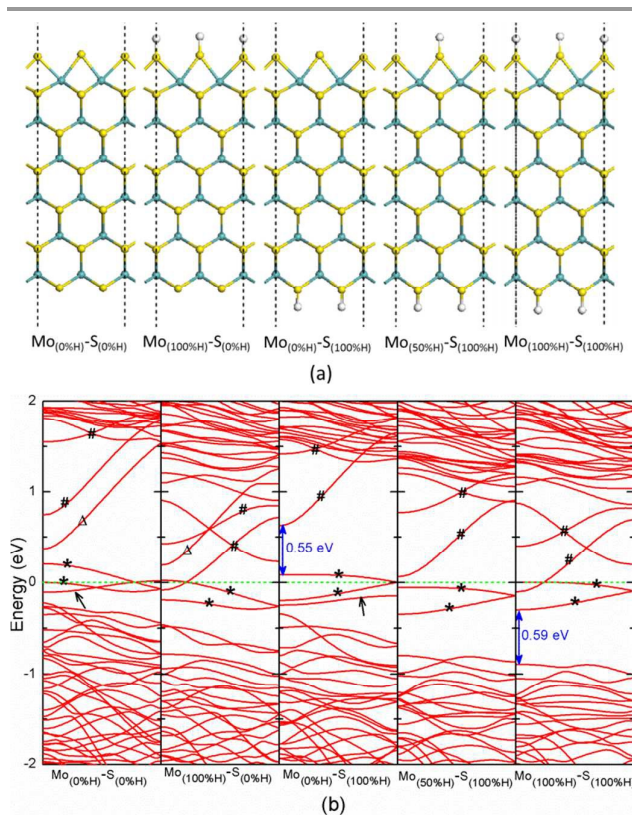


Fig. 7. (a) Geometric structures of NR-1 with various edge hydrogenation, in which the dashed lines mark the dimension of the unit cell in the x-direction, and (b) corresponding to their energy bands. The Fermi level is set as zero.

Hydrogenation

The hydrogenation of materials is the simplest way of modification, whose mechanism can be significant for band engineering and catalyzing HER.⁵² Finally, we consider an ensemble, the model of NR-1, which can be saturated with different edge hydrogenation, and their optimal structures are shown in Fig. 7(a). As their energy bands shown in Fig. 7(b), it is observed that $\text{Mo}_{(0\%)(\text{H})}\text{-S}_{(0\%)(\text{H})}$ is accompanied with sharp mid-

gap states while $\text{Mo}_{(0\%)\text{H}}\text{-S}_{(100\%)\text{H}}/\text{Mo}_{(100\%)\text{H}}\text{-S}_{(100\%)\text{H}}$ has the characteristic like p/n -type semiconducting behaviour. In addition, it should be considered that the energy gaps calculated by DFT are generally underestimated compared with experimentally obtained ones. Among them, $\text{Mo}_{(100\%)\text{H}}\text{-S}_{(0\%)\text{H}}$ is the highest metallic. The transition of electronic structures from $\text{Mo}_{(0\%)\text{H}}\text{-S}_{(0\%)\text{H}}$ to $\text{Mo}_{(0\%)\text{H}}\text{-S}_{(100\%)\text{H}}$ can be explained by the disappearance of one band marked by triangle above the Fermi level owing to S-edge hydrogenation. Noticeably, we also observe that a flat band introduced by Mo-edge atoms at the Fermi level indicated by arrow disappears after Mo-edge hydrogenation. The prominent edge states from this flat band can trap other electronic states from Mo-edge atoms. Thereby, its disappearance will lead to other bands attributed to Mo-edge atoms approaching the Fermi level, which are marked by pound sign in Fig. 7(b). Such bands are dispersed and have a tendency to couple with electronic states of S-edge atoms. In addition, due to S-edge hydrogenation, the edge S atoms at the S-edge are no longer responsible for two apparent bands at the Fermi level. Instead, such bands marked by asterisk are induced by Mo atoms at the S-edge, which can be understood in the middle panel of ESI Fig. S6. Consequently, it prompts that the Fermi level is lifted up, and n-type semiconductor ($\text{Mo}_{(100\%)\text{H}}\text{-S}_{(100\%)\text{H}}$) is achieved by two-edge hydrogenation.

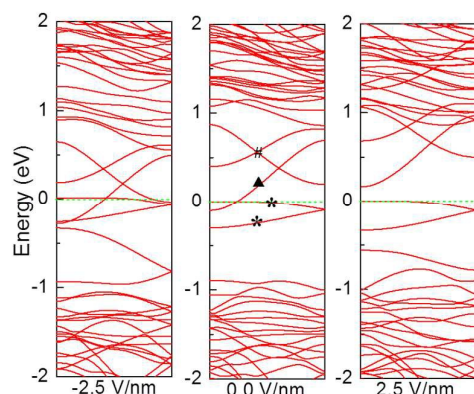


Fig. 8. The energy bands of hydrogen passivated NR-1 ($\text{Mo}_{(100\%)\text{H}}\text{-S}_{(100\%)\text{H}}$) under E_{ext} are exhibited. The Fermi level is set as zero.

We now pay attention to E_{ext} effects on electronic structures of nanoribbon with edge hydrogenation. We take the configuration of $\text{Mo}_{(100\%)\text{H}}\text{-S}_{(100\%)\text{H}}$ as an example. As shown in the middle panel of Fig. 8, there are five energy bands around the Fermi level. Among them, one band marked by triangle originating from Mo atoms at the Mo-edge extends down and goes across the Fermi level. It will hybridize with bands coming from Mo atoms at the S-edge marked by asterisk at the Fermi level. Another two bands form the relatively shallower states marked by pound sign, and lie above the Fermi level. When the positive or negative E_{ext} is applied, we observe that the bands marked by triangle and pound signs shift up or down apparently. Similar to those of bare NR-1, the energy bands contributed from Mo-edge atoms are greatly sensitive to E_{ext} for hydrogenation NR-1. Additionally, it is noted that one

valence band visibly extends up under E_{ext} , and thus energy gap is reduced. Under $E_{\text{ext}} = -2.5$ V/nm, it almost connects with bands at the Fermi level. The E_{ext} can change $\text{Mo}_{(100\%)\text{H}}\text{-S}_{(100\%)\text{H}}$ from n-type semiconductor into metal, especially for wider nanoribbons in ESI Fig. S7.

It has been predicted that the HER activity arises from the Mo-edge for MoS_2 .⁴⁰ The HER requires that the adsorption energy of H at the Mo-edge should be in an appropriate range. If H binds very strong to the edge, the H release step will be slow. If H does not bind to the edge, the proton/electron-transfer step will not occur. Thus, they will eventually lead to decreases the HER activity. Interestingly, at the shallower states above the Fermi level, we find that a characteristic of anti-bonding orbitals appears between the orbital wavefunctions of H and S at the Mo-edge as shown in the inset of Fig. 9. We suggest that the anti-bonding orbitals near the Fermi level could result in a notably weaker interaction between H and edge atom, thus leading to H desorption relatively easily.⁵³ Applying E_{ext} , DOS and energies of anti-bonding orbitals are shown in ESI Fig. S6 and Fig. S8. LDOS of H atom at the Mo-edge have also been calculated as a function of ribbon width under E_{ext} in ESI Fig. S9. Through analyzing these results, we find that E_{ext} can modulate the energy of anti-bonding orbitals. As above description, the E_{ext} can result in the charge redistribution, which has an apparent influence on Mo-edge states. The positive E_{ext} can increase the energy of anti-bonding orbitals, far away from the Fermi level. Thus, it will lead to high energy barrier for H release. On the contrary, the negative E_{ext} will cause H desorption to be relatively easy. It is believed that the E_{ext} may tune the adsorption behavior of H atoms at the Mo-edge, resulting in an enhanced HER activity of edge sites. At the same time, the energy gap of nanoribbon can also be reduced under E_{ext} in Fig. 8 and ESI Fig. S7, leading to an increased electric conductivity. Besides the aspect of active sites, a high conductivity ensures a fast electron transport and facilitates the combination between positive protons and catalysts. Consequently, we suggest that these two factors can possibly be regulated and synergistically improve the HER performance.

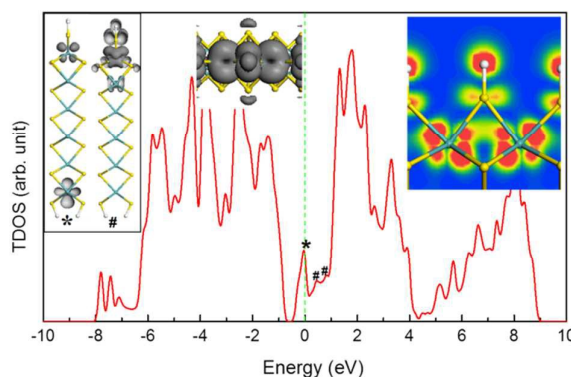


Fig. 9. TDOS of hydrogen passivated NR-1 ($\text{Mo}_{(100\%)\text{H}}\text{-S}_{(100\%)\text{H}}$) under $E_{\text{ext}} = 0.0$ V/nm. Inset: the electronic states near the Fermi level. The Fermi level is set as zero. The isosurface value is 0.02 electrons/ au^3 .

Conclusions

According to experimental HAADF and HR-TEM images of needle-like MoS₂ nanowires and ultranarrow MoS₂ nanoribbons, the models of MoS₂ nanoribbons are constructed. Their electronic structures are investigated in detail using DFT. Compared with semiconducting MoS₂ monolayer, the extra electronic states are introduced by edge atoms into the gap, and thus they exhibit metallic characteristic. We discriminated and identified these extra states according to major contributors to them. It is found that such states induced by edge atoms are sensitive to E_{ext} , viz., the electronic states around the Fermi level shift up or down when the positive or negative E_{ext} is applied. It can be explained by the charge redistribution in the MoS₂ nanoribbon under E_{ext} . The electronic structures of nanoribbon can vary with different edge hydrogenation. Moreover, after edge hydrogenation, we observe a characteristic of anti-bonding orbitals between the orbital wavefunctions of H and S at Mo-edge. It is interesting that the energy of anti-bonding orbitals and electric conductivity of nanoribbon can be tailored by E_{ext} . Therefore, it is suggested that a means of controlling HER activity may be provided.

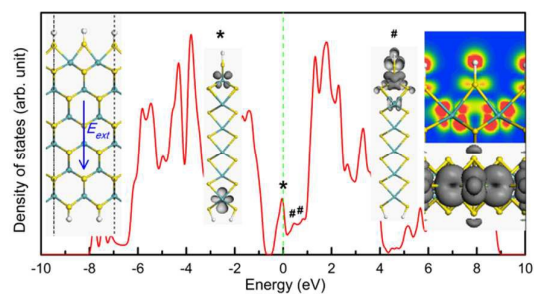
Acknowledgements

The authors would like to thank the financial supports from National Natural Science Foundation of China (Grant No. 51372095), Program for Changjiang Scholars and Innovative Research Team in University (PCSIRT), and the "211" and "985" project of Jilin University.

Notes and references

- K.S. Novoselov, A.K. Geim, S.V. Morozov, D. Jiang, and Y. Zhang, *Science*, 2004, **306**, 666.
- Q. Tang and Z. Zhou, *Prog. Mater. Sci.*, 2013, **58**, 1244.
- Q. Tang, Z. Zhou and Z.F. Chen, *WIREs Comput. Mol. Sci.*, 2015, **5**, 360.
- K.S. Novoselov, D. Jiang, F. Schedin, T.J. Booth, V.V. Khotkevich and S.V. Morozov, *Proc. Natl. Acad. Sci. USA*, 2005, **102**, 10451.
- A. Ueno, T. Fujita, M. Matsue, H. Yanagisawa, C. Oshima, F. Patthey, H.-C. Ploigt, W.-D. Schneider and S. Otani, *Surf. Sci.*, 2006, **600**, 3518.
- P. Amo-Ochoa, L. Welte, R. González-Prieto, P.J. Sanz Miguel, C.J. Gómez-García, E. Mateo-Martí, S. Delgado J. Gómez-Herrero and F. Zamora, *Chem. Commun.* 2010, **46**, 3262.
- M. Naguib, M. Kurtogly, V. Presser, J. Lu, J. Niu, M. Heon, L. Hultman, Y. Gogotsi and M.W. Barsoum, *Adv. Mater.*, 2011, **23**, 4248.
- M. Naguib, O. Mashtalir, J. Carle, V. Presser, J. Lu, L. Hultman, Y. Gogotsi and M.W. Barsoum, *ACS Nano*, 2012, **6**, 1322.
- D. Jose and A. Datta, *Acc. Chem. Res.*, 2014, **47**, 593.
- S.L. Zhang, M.Q. Xie, F.Y. Li, Z. Yan, Y.F. Li, E.J. Kan, W. Liu, Z.F. Chen and H.B. Zeng, *Angew. Chem. Int. Ed.*, DOI: 10.1002/anie.201507568.
- K.F. Mak, C. Lee, J. Hone, J. Shan and T.F. Heinz, *Phys. Rev. Lett.*, 2010, **105**, 136805.
- M. Chhowalla, H.S. Shin, G. Eda, L.J. Li, K.P. Loh and H. Zhang, *Nature Chem.*, 2013, **5**, 263.
- M.V. Bollinger, J.V. Lauritsen, K.W. Jacobsen, J.K. Nørskov, S. Helveg and F. Besenbacher, *Phys. Rev. Lett.*, 2001, **87**, 196803.
- M.Y. Han, B. Ozyilmaz, Y.B. Zhang and P. Kim, *Phys. Rev. Lett.*, 2007, **98**, 206805.
- Y.F. Li, Z. Zhou, S.B. Zhang and Z.F. Chen, *J. Am. Chem. Soc.*, 2008, **130**, 16739.
- K. Dolui, C.D. Pemmaraju and S. Sanvito, *ACS Nano*, 2012, **6**, 4823.
- L.Z. Kou, C. Tang, Y. Zhang, T. Heine and T. Frauenheim, *J. Phys. Chem. Lett.*, 2012, **3**, 2934.
- Z.Y. Wang, H. Li, Z. Liu, Z.J. Shi, J. Lu, K. Suenaga, S.-K. Joong, T. Okazaki, Z.N. Gu, J. Zhou, Z.X. Gao, G.P. Li, S. Sanvito, E.G. Wang and S. Lijima, *J. Am. Chem. Soc.*, 2010, **132**, 13840.
- A. Splendiani, L. Sun, Y.B. Zhang, T.S. Li, J.H. Kim, C.Y. Chim, G. Galli and F. Wang, *Nano Lett.*, 2010, **10**, 1271.
- B. Radisavljevic, A. Radenovic, J. Brivio, V. Giacometti and A. Kis, *Nat. Nanotechnol.*, 2011, **6**, 147.
- B. Radisavljevic, M.B. Whitwick and A. Kis, *Appl. Phys. Lett.*, 2012, **101**, 043103.
- X.Q. Deng, Z.H. Zhang, G.P. Tang, Z.Q. Fan and C.H. Yang, *Carbon*, 2014, **66**, 646.
- A.R. Botello-Mendez, F. Lopez-Urias, M. Terrones and H. Terrnoes, *Nanotechnology*, 2009, **20**, 325703.
- C. Ataca, H. Şahin, E. Aktürk and S. Ciraci, *J. Phys. Chem. C*, 2011, **115**, 3934.
- H. Pan and Y.W. Zhang, *J. Mater. Chem.*, 2012, **22**, 7280.
- Z. Qi, P. Cao and H.S. Park, *J. Appl. Phys.*, 2013, **114**, 163508.
- Y.F. Li, D.H. Wu, Z. Zhou, C.R. Cabrera and Z.F. Chen, *J. Phys. Chem. Lett.*, 2012, **3**, 2221.
- C. Ataca, H. Şahin, E. Aktürk and S. Ciraci, *J. Phys. Chem. C*, 2011, **115**, 3934.
- H. Pan and Y.W. Zhang, *J. Phys. Chem. C*, 2012, **116**, 11752.
- L. Zhang, L.H. Wan, Y.J. Yu, B. Wang, F.M. Xu, Y.D. Wei and Y. Zhao, *J. Phys. Chem. C*, 2015, **119**, 22164.
- Y. Han, J. Zhou and J.M. Dong, *Appl. Surf. Sci.* 2015, **346**, 470.
- Y.W. Son, M.L. Cohen and S.G. Louie, *Nature*, 2006, **444**, 347.
- Q. Yue, S.L. Chang, J. Kang, X.A. Zhang, Z.Z. Shao, S.Q. Qin and J.B. Li, *J. Phys.: Condens. Matter*, 2012, **24**, 335501.
- Q.H. Liu, L.Z. Li, Y.F. Li, Z.X. Gao, Z.F. Chen and J. Lu, *J. Phys. Chem. C*, 2012, **116**, 21556.
- X.G. Liu and Z.Y. Li, *J. Phys. Chem. Lett.*, 2015, **6**, 3269.
- G.A. Camacho-Bragado, J.L. Elechiguerra, A. Olivas, S. Fuentes, D. Galvan and M. J. Yacamán, *J. Catal.*, 2005, **234**, 182.
- D.H. Galvan, A. P. Amarillas and M. José-Yacamán, *Catal. Lett.*, 2009, **132**, 323.
- P. Paybaud, J. Hafner, G. Kresse, S. Kasztelan and H. Toulhoat, *J. Catal.* 2000, **189**, 129.
- S. Helveg, J.V. Lauritsen, E. Lægsgaard, I. Stensgaard, J.K. Nørskov, B.S. Clausen, H. Topsøe and F. Besenbacher, *Phys. Rev. Lett.*, 2000, **84**, 951.
- B. Hinnemann, P.G. Moses, J. Bonde, K.P. Jørgensen, J.H. Nielsen, S. Hørch, I. Chorkendorff and J. K. Nørskov, *J. Am. Chem. Soc.*, 2005, **127**, 5308.
- W. Chen, E.J.G. Santos, W.G. Zhu, E. Kaxiras and Z.Y. Zhang, *Nano Lett.*, 2013, **13**, 509.
- J.F. Xie, J.J. Zhang, S. Li, F. Grote, X.D. Zhang, H. Zhang, R.X. Wang, Y. Lei, B.C. Pan and Y. Xie, *J. Am. Chem. Soc.*, 2013, **135**, 17881.
- C. Tsai, K. Chan, J.K. Nørskov and F. Abild-Pedersen, *Catal. Sci. Technol.*, 2015, **5**, 246.
- J. Deng, H.B. Li, J.P. Xiao, Y.C. Tu, D.H. Deng, H.X. Yang, H.F. Tian, J.Q. Li, P.J. Ren and X.H. Bao, *Energy Environ. Sci.*, 2015, **8**, 1594.

- 45 B. Delley, *J. Chem. Phys.*, 1990, **92**, 508; B. Delley, *J. Chem. Phys.*, 2000, **113**, 7756.
- 46 J. P. Perdew, *Phys. Rev. Lett.*, 1996, **77**, 3865.
- 47 E.R. McNellis, J. Meyer and K. Reuter, *Phys. Rev. B*, 2009, **80**, 205414.
- 48 G. Kresse, J. Furthmuller, *Phys. Rev. B*, 1996, **54**, 11169.
- 49 A. Nijamudheen, R. Bhattacharjee, S. Choudhury and A. Datta, *J. Phys. Chem. C*, 2015, **119**, 3802.
- 50 Y. Ma, Y. Dai, M. Guo, C. Niu, Y. Zhu and B. Huang, *ACS Nano*, 2012, **6**, 1695.
- 51 C.Q. Sun, *Prog. Solid State Chem.*, 2007, **35**, 1.
- 52 D. Jose and A. Data, *Phys. Chem. Chem. Phys.*, 2011, **13**, 7304.
- 53 H.A. Aleksandrov, S.M. Kozlov, S. Schauermaun, G.N. Vayssilov and K.M. Neyman, *Angew. Chem. Int. Ed.*, 2014, **53**, 13371-13375.



E_{ext} can tune the interaction between H and edge, and at the same time enhance the intrinsic conductivity of nanoribbon.